RSC Advances

PAPER

View Article Online
View Journal | View Issue

Cite this: *RSC Adv.*, 2020, **10**, 7126

Heating-up synthesis of cesium bismuth bromide perovskite nanocrystals with tailored composition, morphology, and optical properties†

Donguk Lee,[a] MinHye Kim,[a] Ho-Young Woo,[a] Jiyeon Chae,[a] Dawon Lee,[a] Sanghyun Jeon,[b] Soong Ju Oh *[b] and Taejong Paik *[a]

Received 3rd December 2019
Accepted 8th February 2020

DOI: 10.1039/c9ra10106c

rsc.li/rsc-advances

This study represents the heating-up synthesis of lead-free cesium bismuth bromide perovskite nanocrystals (NCs). CsBr and $BiBr_3$ precursors are used to synthesize uniform and phase-pure cesium bismuth bromide NCs, and the reaction is performed *via* an injection-free, heating-up method in the presence of a solvent mixture with a high boiling point. The size and composition of cesium bismuth bromide NCs are readily controlled by changing the reaction time, temperature, and amount of surfactant added to the reaction mixture. Upon heating, sequential phase evolution occurs, resulting in the formation of kinetically stable BiOBr in the early reaction stages, which transformed into the thermodynamically stable Cs_3BiBr_6 and $Cs_3Bi_2Br_9$ with an increase in either the reaction time or the reaction temperature. Furthermore, the absorption and photoluminescence properties of Cs_3BiBr_6 and $Cs_3Bi_2Br_9$ NCs are characterized to investigate their composition-dependent optical properties. This work provides the potential to synthesize various types of lead-free perovskite NCs by tailoring the size and compositions.

Introduction

Halide perovskites with an ABX_3 (A, B = cation, X = halide) structure have been extensively studied for application to electronic and optoelectronic devices.[1–3] Perovskite nanocrystals (NCs) in particular have attracted much attention owing to their unique photoluminescence (PL) properties.[4,5] Perovskite NC band gaps are tunable by changing the size, shape, and compositions of the NCs,[6,7] which enables the tailoring of the absorption and emission wavelengths of the NCs. Among a variety of perovskite NCs, lead-based perovskite NCs are particularly interesting owing to their outstanding luminescent properties.[8,9] Lead-halide perovskite NCs exhibit very high photoluminescence quantum yields (PLQYs), at higher than 90%,[10] narrow absorption and emission band widths (FWHM is 12–25 nm) owing to the quantum confinement effect,[11,12] and short fluorescence lifetimes.[13,14] In addition, the size, shape, and compositions of these NCs can be easily changed by controlling the reaction parameters[15–18] and post-synthetic treatments;[19–25] this allows for the facile management of spectral conversion. However, despite this outstanding potential, lead-based perovskite NCs have heavy metal composition, which makes it potentially toxic to the environment and human health.[26] Therefore, many researchers have made considerable effort to develop lead-free perovskite NCs with superior optical properties.

Various lead-free perovskite NCs using tin,[27,28] bismuth,[29–32] and antimony,[33,34] have been investigated. Among them, Bi-based perovskite NCs exhibit the potential for stability and environment-friendliness. Bismuth is a less-toxic heavy metal, which reduces concern regarding environmental and health issues for Bi-based NCs.[35] In addition, the luminescent properties of Bi-based perovskite NCs have been tremendously improved along the development of synthetic methods for the preparation of these NCs.[36–38] After Park *et al.* discovered the synthesis of a $A_3Bi_2X_9$ (A = methylammonium or cesium) perovskite structure,[29] the colloidal synthesis of $A_3Bi_2X_9$ NCs using the hot-injection method was demonstrated.[39] Yang *et al.* reported on a ligand-assisted re-precipitation method (LARP) for the synthesis of $Cs_3Bi_2Br_9$ NCs; their method showed a 4.5% PLQY.[40] Moreover, Leng *et al.* synthesized this NC by using ethanol as the antisolvent; the PLQY reached approximately 20% with this method.[41] Recently, the synthesis of cesium bismuth bromide with Cs_3BiBr_6 composition has been reported in the literature.[37,42,43] In addition, many studies have been carried out to improve the stability of perovskite; for instance, the core–shell or double perovskite structure ($A_2BB'X_6$) has been explored.[44] Although various procedures for the preparation of Bi-based perovskite NCs have been developed, synthetic methods to systematically tune the size and shape of Bi-based

[a]*Department of Integrative Engineering, Chung-Ang University, Seoul 06974, Republic of Korea. E-mail: paiktae@cau.ac.kr*

[b]*Department of Materials Science and Engineering, Korea University, Seoul 02841, Republic of Korea. E-mail: sjoh1982@korea.ac.kr*

† Electronic supplementary information (ESI) available. See DOI: 10.1039/c9ra10106c

perovskite NCs and methods to tailor their optical properties have been rarely studied.

Among the various types of colloidal synthetic methods, the heating-up process for the synthesis of inorganic NCs has been widely studied.[45–47] The heating-up method is a one-pot and injection-free process designed to synthesize highly uniform NCs and to tailor the sizes and shapes of the NCs.[48] In this process, metal precursors and solvents are placed in reaction vessels and the reaction temperatures increases. At the high temperature, the nucleation and growth of NCs is induced to form crystalline NCs. Since such a high temperature injection process is typically not used in synthesis, the heating-up method offers a relatively safe and controllable synthetic process, which is potentially beneficial for mass production. Various types of NCs are synthesized using the heating-up process; for example, metal oxide,[49,50] metal chalcogenides,[51,52] and lanthanide NCs.[53,54] Many literatures note that the size and shape of NCs can be easily controlled by changing reaction parameters such as reaction time[55] and temperature,[56,57] types of metal precursors,[47] and the presence of shape directing reagent[58–61] during preparation. Despite the various advantages of the heating-up process, heating-up process to synthesize bismuth perovskite NCs has not been extensively studied thus far. In addition, there are very few papers on controlling the size and shape of perovskite NCs using the heating-up process.

In this paper, we demonstrate a method of injection-free heating-up synthesis of cesium bismuth bromide NCs which allows for the tuning of the size, shape, and composition of perovskite NCs. CsBr and $BiBr_3$ precursors are used to synthesize uniform and phase-pure perovskite NCs. We observed that the phase evolution of Bi-based NCs occurs during the heating-up reaction. At the early reaction stages, BiOBr NCs are formed from $BiBr_3$ precursors. In the presence of CsBr at a higher reaction temperature, BiOBr NCs are transformed into Cs_3BiBr_6 phase NCs. With further increase in the reaction temperature, the composition of the NCs transform from Cs_3BiBr_6 to trigonal $Cs_3Bi_2Br_9$ nanoplates (NPs); in contrast, metallic Bi is formed in the absence of CsBr. We demonstrate that the size and shape of $Cs_3Bi_2Br_9$ NCs are tuned by changing the amount of oleic acid added into the reaction solution and by modulating the temperature. In addition, we analyze the optical properties of Cs_3BiBr_6 NCs and $Cs_3Bi_2Br_9$ NPs to understand the effect of the composition of NCs on their photoluminescence.

Experimental section

Chemicals

Cesium bromide (99.999%, trace metals basis), oleic acid (tech, 90%), 1-octadecene (90%) and oleylamine (tech, 70%) were purchased from Sigma-Aldrich and bismuth bromide (97%) was purchased from Alfa Aesar. All chemicals were used without any further purification.

Heating-up synthesis of Cs_3BiBr_6 perovskite NCs

1.072 g of CsBr and 0.252 g of $BiBr_3$ were added to a 100 mL three-necked flask containing 20 mL of 1-octadecene (ODE), 1.5 mL of oleylamine (OM), and 1.5 mL of oleic acid (OA). The reaction mixture was heated to 105 °C and the temperature was maintained for an hour under vacuum to remove volatile solvents. After degassing, the reaction mixture was further heated to 160 °C for the synthesis of perovskite NCs. After 60 min of reaction, the solution was cooled to room temperatures. The reaction mixture was diluted with anhydrous toluene and centrifuged at 3000 rpm for 15 s to precipitate unreacted cesium bromide and BiOBr nanoplate byproducts. After precipitates were discarded, the perovskite NCs were collected using centrifugation at 8000 rpm and 3 min.

Heating-up synthesis of $Cs_3Bi_2Br_9$ perovskite NPs

For the synthesis of large sized NCs, 15 mL of OA, 1.5 mL of OM, and 7.5 mL of ODE were added to the reaction mixtures and the synthesis was performed under the same conditions as the aforementioned experiment.

Synthesis of pure BiOBr NPs

All reactants and processes were the same as those used in the synthesis of cesium bismuth bromide perovskite NCs, except that CsBr was absent. 0.252 g of $BiBr_3$, 20 mL of ODE, 1.5 mL of OM and 1.5 mL of OA were loaded into a 100 mL three-neck flask. The mixture was then heated to 105 °C under vacuum for 1 h. After this, the mixture was heated to 135 °C and this temperature was maintained for 1 h to form BiOBr nanoplates. The nanoparticles were purified with toluene and methanol, and hexane was used as the storage solvent.

Characterization

Transmission electron microscopy (TEM) images were recorded by a JEOL JEM-2100 operating at 200 kV. High-Resolution Transmission Electron Microscopy (HRTEM) images were collected by a JEOL-F200 and JEOL JEM-3010. Energy Dispersive X-ray Spectroscopy (EDS) measurement and mapping were performed using JEOL JEM-ARM200F. Scanning electron microscopy (SEM) images were recorded using Carl Zeiss SIGMA operating at 5 kV. X-ray diffraction (XRD) was conducted using Bruker-AXS New D8-Advance. X-ray photoelectron spectroscopy (XPS) measurements were performed using Thermo-Fisher Scientific K-alpha. Absorption and transmission spectra were collected with a JASCO V-770 UV-VIS-NIR spectrometer. Photoluminescence (PL) spectra were obtained using EDINBURGH FS5. The PLQY was measured using a fluorimeter equipped with an integrating sphere. Time-resolved photoluminescence decay data were collected using a HORIBA Fluorolog-3 with a single photon-counting photomultiplier tube (PMT) under a 374 nm pulsed laser diode.

Result and discussion

Colloidal cesium bismuth bromide perovskite NCs are prepared *via* heating-up synthesis using CsBr and $BiBr_3$ precursors. In this experiment, $BiBr_3$ and CsBr are added together into the reaction mixture with an excess of Cs precursors. As CsBr does not completely dissolve in the ODE, OM, and OA solvent

mixture, the reaction is conducted between solid-phase CsBr and dissolved $BiBr_3$ in the solution. Fig. 1a–d displays TEM images of the cesium bismuth bromide NCs. The low-magnification image shows the monodisperse cesium bismuth bromide NCs with a narrow size distribution. The size of the cesium bismuth bromide NCs is 14.22 nm $\pm$ 1.72 nm, as calculated by statistical size analysis of the TEM images. The cesium bismuth bromide NCs are linearly arrayed into one-dimensional chains, as displayed in Fig. 1a and b. At the same time, the one-dimensional chains are also self-assembled into close-packed structures to form extended two-dimensional superlattice arrays (Fig. 1c and d). HRTEM images show single-crystalline structures of the cesium bismuth bromide NCs (Fig. 1e). Fig. 1f shows the XRD pattern of the cesium bismuth bromide NCs. The XRD pattern is very similar to that of the Cs_3BiBr_6 composition reported in the recent literature.[37,42,43] The STEM-EDS analysis also reveals the composition of the Cs_3BiBr_6 NCs. Fig. 1g shows the dark-field TEM image of the Cs_3BiBr_6 NCs, and Fig. 1h–j are the STEM-EDS elemental mapping images, which exhibit a homogeneous elemental distribution of Cs, Bi, and Br in the NCs. The relative ratio of Cs : Bi : Br atoms is 34.96 : 11.18 : 53.86, which reveals that the composition of the as-synthesized NCs is Cs_3BiBr_6.

The synthesis of cesium bismuth bromide with the composition Cs_3BiBr_6 is readily controlled by increasing the amount of OA added into the reaction mixture. As the amount of OA increases from 1.5 mL to 15 mL, two-dimensional $Cs_3Bi_2Br_9$ NPs are synthesized. Fig. 2a shows TEM images of the $Cs_3Bi_2Br_9$ NPs. The size of the $Cs_3Bi_2Br_9$ NPs is approximately 200–400 nm. HRTEM images show the single-crystalline structure of a $Cs_3Bi_2Br_9$ nanoplate (Fig. 2d and S2, ESI†). Fast Fourier Transform (FFT) patterns of the HRTEM image exhibit hexagonal symmetry, representing the trigonal structure of the $Cs_3Bi_2Br_9$ NPs (Fig. 2d, inset). The STEM-EDS elemental mapping image exhibits a homogeneous elemental distribution of Cs, Bi, and Br in the NPs. The XRD patterns also indicate the trigonal diffraction of the $Cs_3Bi_2Br_9$ NPs (JCPDS no. 44-0714, Fig. 2i). Compositional information is further confirmed by XPS measurements. XPS profiles confirm that the $Cs_3Bi_2Br_9$ NPs comprise Cs, Bi, and Br (Fig. 2j–l).

During the heating-up process, gradual color change of the reaction solution is observed. When 1.5 mL of OA is used for the reaction, the color of the solution is transparent up to 105 °C. Upon heating, the solution color changes to white at approximately 135 °C and then changes to bright yellow at 160 °C, indicating the formation of Cs_3BiBr_6 NCs. In order to understand the growth mechanism of perovskite NCs during the

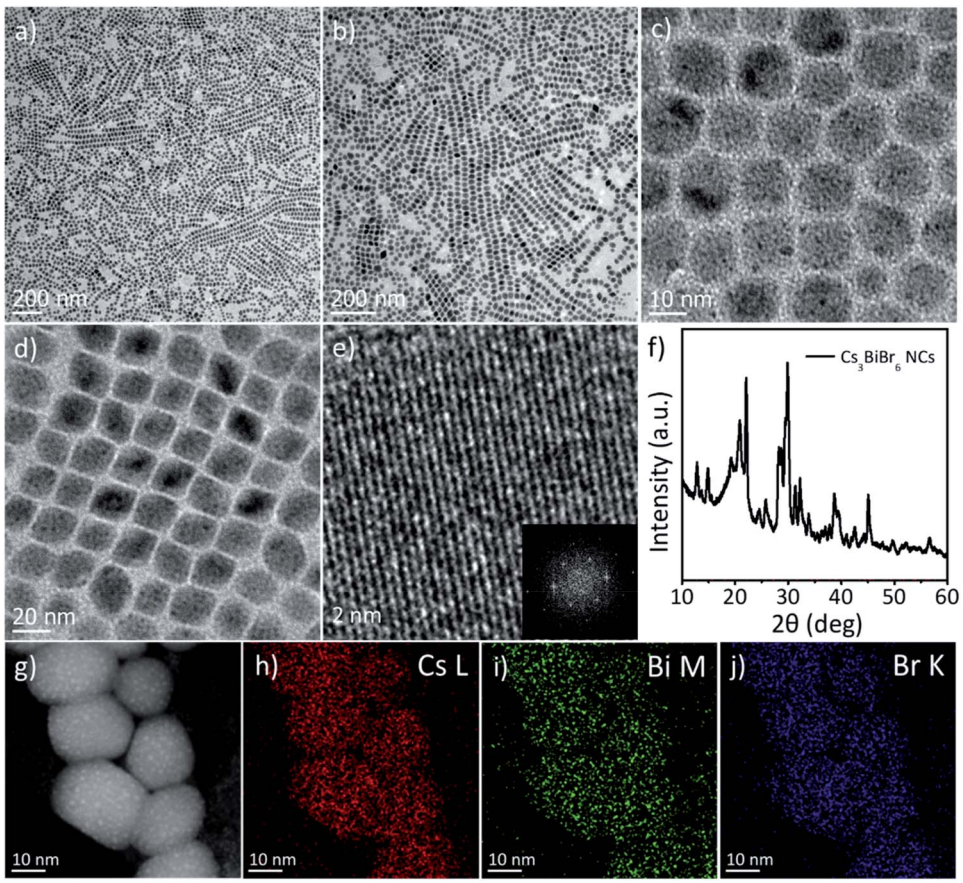

Fig. 1 (a and b) Low-magnification and (c and d) high-magnification TEM images of colloidal Cs_3BiBr_6 NCs, (e) high-resolution TEM image and FFT image of Cs_3BiBr_6 NCs, (inset) (f) XRD pattern of Cs_3BiBr_6 NCs. (g) Dark-field TEM image of Cs_3BiBr_6 NCs. (h–j) STEM-EDS mapping of Cs_3BiBr_6 NCs.

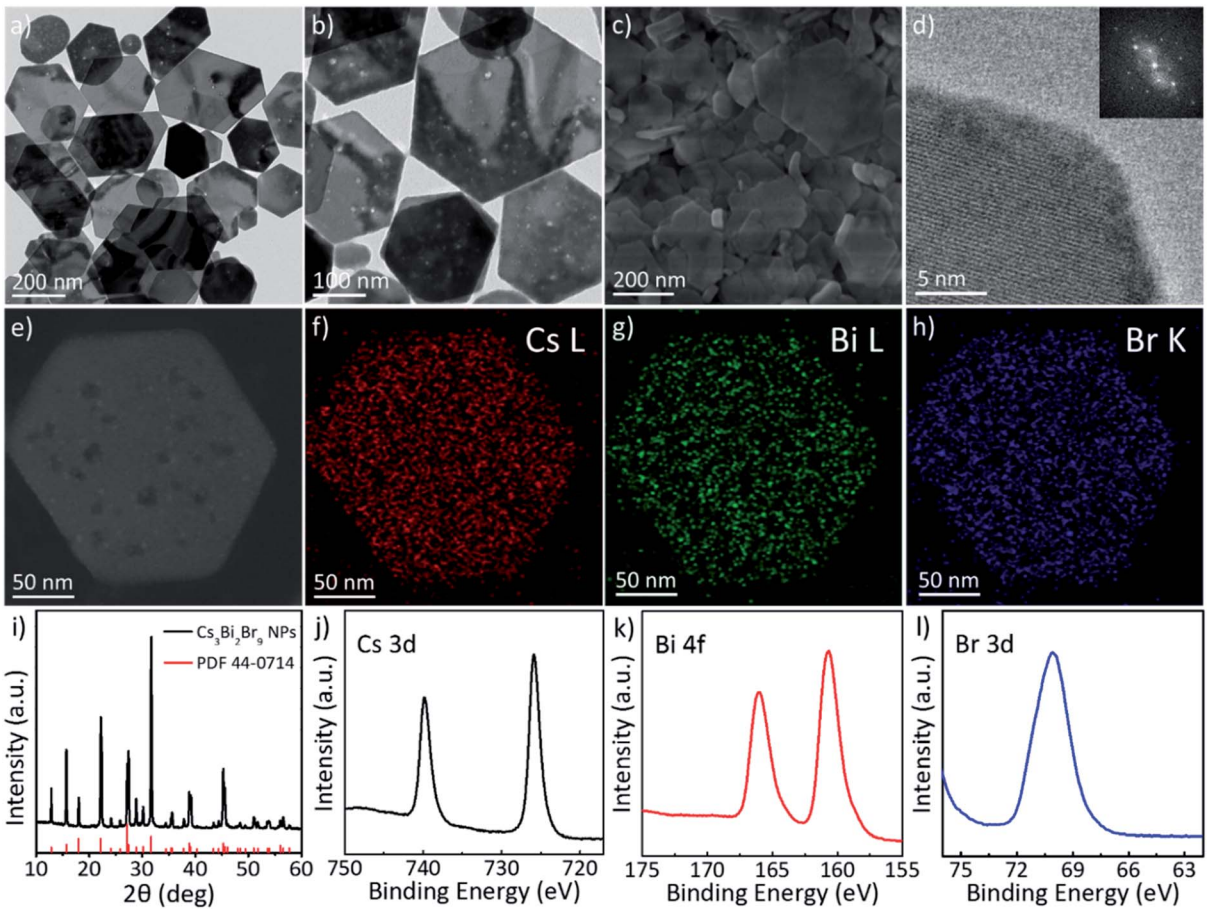

Fig. 2 (a) low-magnification, (b) high-magnification TEM images and (c) SEM image of $Cs_3Bi_2Br_9$ NPs. (d) HRTEM image of $Cs_3Bi_2Br_9$ NPs. (e) Dark-field TEM image of $Cs_3Bi_2Br_9$ NPs. (f–h) EDS mapping of $Cs_3Bi_2Br_9$ NPs. (i) XRD patterns of trigonal $Cs_3Bi_2Br_9$ NPs. (j–l) XPS profiles of $Cs_3Bi_2Br_9$ NPs.

heating-up process, we systematically varied the reaction temperature and investigated the crystal structure of the as-synthesized NCs. When the reaction is performed at 135 °C in the presence of 1.5 mL of OA, BiOBr NPs are formed as a final white product. Fig. S3a–c (ESI†) show TEM and HRTEM images of the BiOBr NPs, which exhibit a rectangular nanoplate morphology. The size of the BiOBr NPs is approximately 25.5 nm. Fig. S3d (ESI†) shows XRD pattern of BiOBr NPs. The XRD pattern reveals pure tetragonal BiOBr phases (JCPDS no. 73-0348). The (101) and (102) diffraction planes are relatively broad compared to the other planes, indicating that the top and bottom surfaces of the nanoplates are (001) planes.

Up to a reaction temperature of 160 °C, the BiOBr NPs are predominantly formed as final products and there is no evidence of reaction between the CsBr and $BiBr_3$ precursors. When the reaction temperature is further increased to over 160 °C, CsBr precursors are involved in the reaction to form slightly yellowish Cs_3BiBr_6 NCs. Cs_3BiBr_6 NCs are predominantly formed at 160 °C with BiOBr NPs as the residual. When the temperature increases to approximately 170 °C, $Cs_3Bi_2Br_9$ NPs are synthesized predominantly, as shown in the XRD patterns (Fig S4, ESI†). The $Cs_3Bi_2Br_9$ NCs are predominantly formed even at a higher reaction temperature, up to 300 °C, without the formation of other phases of Bi-based materials. This reveals that the $Cs_3Bi_2Br_9$ NCs do not transform into the metallic Bi phase even at higher temperatures. This phase transition signifies that BiOBr is a kinetically stable phase and forms in an early reaction stage. In the presence of CsBr, thermodynamically stable Cs_3BiBr_6 NCs are initially formed. When sufficient energy is provided by an increase in the reaction temperature, trigonal phase $Cs_3Bi_2Br_9$ NCs are formed. When the reaction temperature is set above 180 °C while in the absence of CsBr, the reaction solution becomes gray in color, and the XRD pattern indicates that metallic Bi is present, which indicates that the BiOBr phase is reduced to the metallic Bi phase in the absence of CsBr. Even in the presence of CsBr, the Bi phase can appear at a higher temperature and a lower amount of OA in the reaction mixture, which is attributed to the structure transformation from the BiOBr to Bi phases (Fig. S5, ESI†).

To further understand phase evolution from BiOBr NPs to $Cs_3Bi_2Br_9$ NCs during the reaction, aliquots are taken at different time intervals at a fixed temperature and crystal structure is investigated. Fig. 3 displays XRD patterns of the Bi-based NCs taken 15 min from the time interval at 170 °C. The reaction is performed in presence of 1.5 mL of OA. XRD reveals

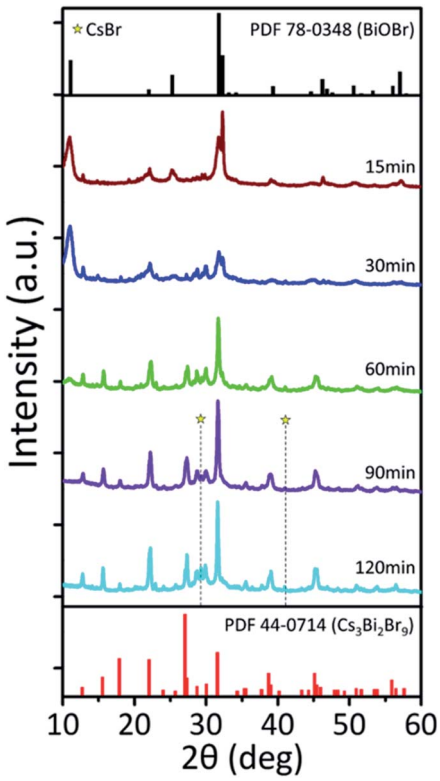

Fig. 3 Reaction time-dependent phase evolution. XRD patterns of Bi-based NCs synthesized at 170 °C with different time intervals.

that BiOBr is predominantly formed during the early stages of the reaction. After 60 minutes of reaction, phase transformation from BiOBr NPs to $Cs_3Bi_2Br_9$ NCs occurs to form the mixture of BiOBr and $Cs_3Bi_2Br_9$ NCs. As the reactions are performed at 170 °C, the Cs_3BiBr_6 phase is not indicated by the XRD patterns. After 90 minutes of reaction, BiOBr NPs are completely converted into $Cs_3Bi_2Br_9$ NCs. This trend confirms that the kinetically stable BiOBr forms in the early stage of the reaction and is then transformed into $Cs_3Bi_2Br_9$ NCs, as illustrated in Fig. 4. Since much smaller Cs_3BiBr_6 NCs are formed from BiOBr NPs

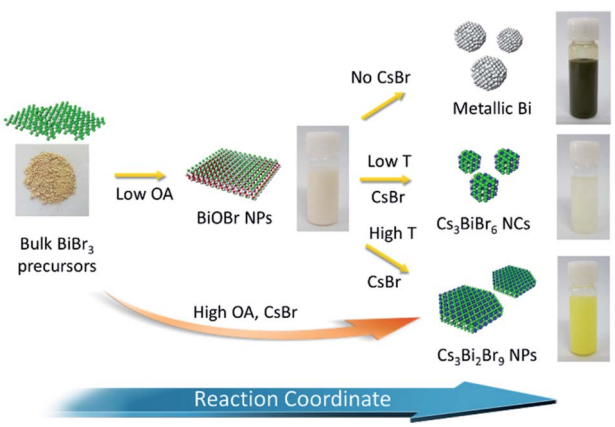

Fig. 4 A schematic representation of the formation of Cs_3BiBr_6 NCs and $Cs_3Bi_2Br_9$ NPs from $BiBr_3$ and CsBr precursors.

during the phase transformation, Cs_3BiBr_6 NCs are formed while dissolution of BiOBr NPs occurs. We also observed that the amount of OA plays an important role in the phase transition during the reaction. As the amount of OA increases, the Cs_3BiBr_6 phase is diminished, and $Cs_3Bi_2Br_9$ forms at a lower reaction temperature. In the presence of 1.5 mL of OA, $Cs_3Bi_2Br_9$ NCs begin to form at 170 °C. When the amount of OA increases to 15 mL, the reaction solution turns yellow even below 100 °C (Fig. S6, ESI†), which is lower than the formation temperature of BiOBr (Fig. 4). This indicating that the presence of OA facilitates the formation of $Cs_3Bi_2Br_9$ NPs, which may be attributed to the interaction between OA surfactants and CsBr salts promoting the dissolution of CsBr salts in the non-polar solvent. The ratio of Bi precursors to Cs precursors is an important parameter to control the growth of $Cs_3Bi_2Br_9$ NCs. As CsBr is not completely soluble in non-polar solvents, excess CsBr is added to facilitate the growth of NCs during the reaction, instead of adding a stoichiometric amount of the CsBr precursors. If Cs and Bi are used at a stoichiometric ratio, the phase transformation of BiOBr to $Cs_3Bi_2Br_9$ is delayed and a relatively large amount of BiOBr remains as a final product.

We investigated the composition-dependent optical properties of Cs_3BiBr_6 NCs and $Cs_3Bi_2Br_9$ NPs. Fig. 5a displays the absorption spectra of the small Cs_3BiBr_6 NCs and large $Cs_3Bi_2Br_9$ perovskite NPs. Band absorption spectra in blue is observed in the UV region. The band gap of large $Cs_3Bi_2Br_9$ is

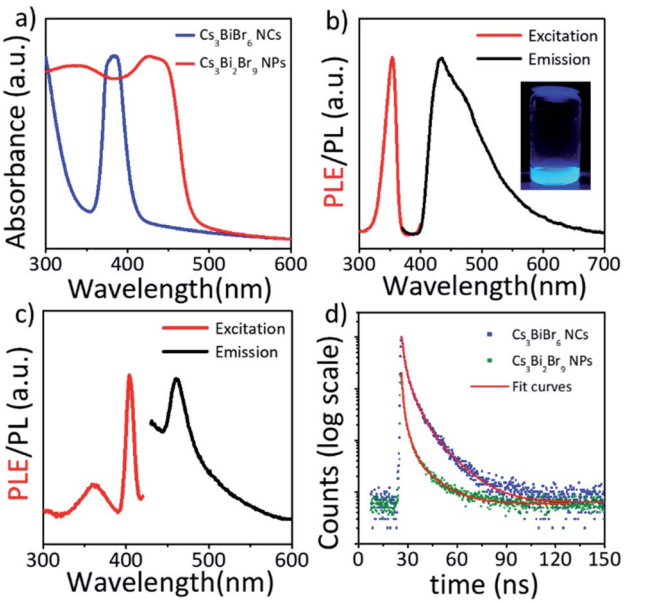

Fig. 5 Optical properties of Cs_3BiBr_6 NCs and $Cs_3Bi_2Br_9$ NPs. (a) Absorption spectrum of Cs_3BiBr_6 NCs (blue) and $Cs_3Bi_2Br_9$ NPs (red). (b) Excitation and emission spectrum of Cs_3BiBr_6 NCs. Emission spectra is collected under an excitation wavelength of 360 nm and the excitation spectra is measured under an emission wavelength of 440 nm. (c) Excitation and emission spectra of $Cs_3Bi_2Br_9$ NPs. Emission spectra is collected under an excitation wavelength of 358 nm and the excitation spectra is measured under an emission wavelength of 461 nm. (d) Time-resolved photoluminescence decay of Cs_3BiBr_6 NCs (blue) and $Cs_3Bi_2Br_9$ NPs (red) under 374 nm excitation.

2.67 eV (464 nm), which is close to the band gap of bulk $Cs_3Bi_2Br_9$.[31] On the other hand, strong blue-shift of the band gap is observed for smaller Cs_3BiBr_6 NCs. Compared to $Cs_3Bi_2Br_9$ NPs, the onset of the absorption band-edge is blue-shifted to 3.05 eV (406 nm), indicating an increased optical band-gap in addition, very narrow first excitonic absorption is observed at 383.5 nm of peak position. We also characterize the PL properties of Cs_3BiBr_6 NCs and $Cs_3Bi_2Br_9$ NPs. Fig. 5b and c exhibit the excitation and emission spectra of Cs_3BiBr_6 NCs and $Cs_3Bi_2Br_9$ NPs, respectively. While large $Cs_3Bi_2Br_9$ NPs show weak photoluminescence properties, with an emission maximum of 461 nm, deep blue luminescence is observed in small Cs_3BiBr_6 NCs, with an emission maximum of 435 nm. The PLQY of Cs_3BiBr_6 NCs is measured as 6.03%, which is one of the highest values among solvothermally synthesized Cs_3BiBr_6 NCs without further treatments. Fig. 5d shows the PL decay curves of Cs_3BiBr_6 NCs and $Cs_3Bi_2Br_9$ NPs. Time-resolved PL decays are monitored at 440 nm and 461 nm for Cs_3BiBr_6 NCs and $Cs_3Bi_2Br_9$ NPs, respectively, under 374 nm of excitation. All decay curves were fitted according to bi-exponential functions, and the fitting results are listed in Table S1.† The PL decay is attributed to sub-bandgap transition, charge carrier recombination processes, and sub-bandgap state emission (trap emission).[40,62–64] The PL decay of Cs_3BiBr_6 NCs is much longer than that of $Cs_3Bi_2Br_9$ NPs, revealing the higher PLQY of Cs_3BiBr_6 *via* radiative recombination (Table S1, ESI†).

Conclusions

In this study, we demonstrate the heating-up synthesis of lead-free cesium bismuth bromide perovskite NCs. The size and composition of perovskite NCs is readily controlled by changing the amount of OA added to the reaction and by adjusting the reaction temperature. In the presence of 1.5 mL of OA, the small Cs_3BiBr_6 NCs are synthesized with uniform size distribution. When the amount of OA added in the reaction or the reaction temperature increases, large $Cs_3Bi_2Br_9$ NPs are obtained as a final product. We systematically investigated the growth mechanism of cesium bismuth bromide NCs during the heating up process. In the presence of 1.5 mL of OA, phase evolution from BiOBr to Cs_3BiBr_6 occurs upon increasing the reaction temperature, as confirmed by XRD and microscopic measurements. Thermodynamically stable $Cs_3Bi_2Br_9$ NPs are formed in higher temperature reactions, with extended reaction times, and by increasing the amount of OA in the reaction mixture. We investigate the optical properties of Cs_3BiBr_6 NCs and $Cs_3Bi_2Br_9$ NPs. The band-gap of small Cs_3BiBr_6 NCs and large $Cs_3Bi_2Br_9$ NPs are 3.05 eV and 2.67 eV, respectively. Blue photoluminescence is observed owing to the presence of small Cs_3BiBr_6 NCs, while large $Cs_3Bi_2Br_9$ NPs show faint photoluminescence properties. Photoluminescence quantum yield of small Cs_3BiBr_6 NCs is 6.03%, which is the highest value of the high-temperature solvothermally synthesized Cs_3BiBr_6 NCs. The heating-up method provides a novel approach for synthesizing perovskite based NCs with readily controlled size, shape, and composition. We believe that our approach provides the potential to synthesize various types of lead-free perovskite NCs.

Conflicts of interest

There are no conflicts to declare.

Acknowledgements

This research was supported by the Creative Materials Discovery Program through the National Research Foundation of Korea (NRF), funded by Ministry of Science and ICT (NRF-2018M3D1A1059001) and by the National Research Foundation of Korea (NRF) grant funded by the Korea government (MSIT) (NRF-2019R1A4A1028700 and NRF-2017R1C1B1005236). It was also supported by the Korea Institute of Energy Technology Evaluation and Planning (KETEP) under a Grant, the Ministry of Trade, Industry & Energy (MOTIE) of the Republic of Korea (No. 20182020109430).

Notes and references

1 M. Xiao, F. Huang, W. Huang, Y. Dkhissi, Y. Zhu, J. Etheridge, A. Gray-Weale, U. Bach, Y. B. Cheng and L. Spiccia, *Angew. Chem., Int. Ed.*, 2014, **53**, 9898–9903.
2 J. Lin, M. Lai, L. Dou, C. S. Kley, H. Chen, F. Peng, J. Sun, D. Lu, S. A. Hawks and C. Xie, *Nat. Mater.*, 2018, **17**, 261.
3 X. Li, Y. Wu, S. Zhang, B. Cai, Y. Gu, J. Song and H. Zeng, *Adv. Funct. Mater.*, 2016, **26**, 2435–2445.
4 S. T. Ha, X. Liu, Q. Zhang, D. Giovanni, T. C. Sum and Q. Xiong, *Adv. Opt. Mater.*, 2014, **2**, 838–844.
5 Q. Lin, A. Armin, R. C. R. Nagiri, P. L. Burn and P. Meredith, *Nat. Photon.*, 2015, **9**, 106.
6 Q. A. Akkerman, S. G. Motti, A. R. Srimath Kandada, E. Mosconi, V. D'Innocenzo, G. Bertoni, S. Marras, B. A. Kamino, L. Miranda and F. De Angelis, *J. Am. Chem. Soc.*, 2016, **138**, 1010–1016.
7 V. D'Innocenzo, A. R. Srimath Kandada, M. De Bastiani, M. Gandini and A. Petrozza, *J. Am. Chem. Soc.*, 2014, **136**, 17730–17733.
8 H.-S. Kim, C.-R. Lee, J.-H. Im, K.-B. Lee, T. Moehl, A. Marchioro, S.-J. Moon, R. Humphry-Baker, J.-H. Yum and J. E. Moser, *Sci. Rep.*, 2012, **2**, 591.
9 D. Zhang, S. W. Eaton, Y. Yu, L. Dou and P. Yang, *J. Am. Chem. Soc.*, 2015, **137**, 9230–9233.
10 L. Protesescu, S. Yakunin, M. I. Bodnarchuk, F. Krieg, R. Caputo, C. H. Hendon, R. X. Yang, A. Walsh and M. V. Kovalenko, *Nano Lett.*, 2015, **15**, 3692–3696.
11 J. H. Song and S. Jeong, *Nano Convergence*, 2017, **4**, 21.
12 J. Butkus, P. Vashishtha, K. Chen, J. K. Gallaher, S. K. K. Prasad, D. Z. Metin, G. Laufersky, N. Gaston, J. E. Halpert and J. M. Hodgkiss, *Chem. Mater.*, 2017, **29**, 3644–3652.
13 G. Li, Z.-K. Tan, D. Di, M. L. Lai, L. Jiang, J. H.-W. Lim, R. H. Friend and N. C. Greenham, *Nano Lett.*, 2015, **15**, 2640–2644.

14 S. Yakunin, L. Protesescu, F. Krieg, M. I. Bodnarchuk, G. Nedelcu, M. Humer, G. De Luca, M. Fiebig, W. Heiss and M. V. Kovalenko, *Nat. Commun.*, 2015, **6**, 8056.
15 Y. Bekenstein, B. A. Koscher, S. W. Eaton, P. Yang and A. P. Alivisatos, *J. Am. Chem. Soc.*, 2015, **137**, 16008–16011.
16 W. Liu, Q. Lin, H. Li, K. Wu, I. Robel, J. M. Pietryga and V. I. Klimov, *J. Am. Chem. Soc.*, 2016, **138**, 14954–14961.
17 S. Sun, D. Yuan, Y. Xu, A. Wang and Z. Deng, *ACS Nano*, 2016, **10**, 3648–3657.
18 H. Liu, Z. Wu, J. Shao, D. Yao, H. Gao, Y. Liu, W. Yu, H. Zhang and B. Yang, *ACS Nano*, 2017, **11**, 2239–2247.
19 S. Bhaumik, S. A. Veldhuis, Y. F. Ng, M. Li, S. K. Muduli, T. C. Sum, B. Damodaran, S. Mhaisalkar and N. Mathews, *Chem. Commun.*, 2016, **52**, 7118–7121.
20 M. Imran, P. Ijaz, D. Baranov, L. Goldoni, U. Petralanda, Q. Akkerman, A. L. Abdelhady, M. Prato, P. Bianchini and I. Infante, *Nano Lett.*, 2018, **18**, 7822–7831.
21 G. Pan, X. Bai, D. Yang, X. Chen, P. Jing, S. Qu, L. Zhang, D. Zhou, J. Zhu and W. Xu, *Nano Lett.*, 2017, **17**, 8005–8011.
22 T. Ahmed, S. Seth and A. Samanta, *Chem. Mater.*, 2018, **30**, 3633–3637.
23 B. Wang, C. Zhang, S. Huang, Z. Li, L. Kong, L. Jin, J. Wang, K. Wu and L. Li, *ACS Appl. Mater. Interfaces*, 2018, **10**, 23303–23310.
24 D. Gao, B. Qiao, Z. Xu, D. Song, P. Song, Z. Liang, Z. Shen, J. Cao, J. Zhang and S. Zhao, *J. Phys. Chem. C*, 2017, **121**, 20387–20395.
25 B. A. Koscher, J. K. Swabeck, N. D. Bronstein and A. P. Alivisatos, *J. Am. Chem. Soc.*, 2017, **139**, 6566–6569.
26 A. H. Slavney, R. W. Smaha, I. C. Smith, A. Jaffe, D. Umeyama and H. I. Karunadasa, *Inorg. Chem.*, 2016, **56**, 46–55.
27 T. C. Jellicoe, J. M. Richter, H. F. Glass, M. Tabachnyk, R. Brady, S. n. E. Dutton, A. Rao, R. H. Friend, D. Credgington and N. C. Greenham, *J. Am. Chem. Soc.*, 2016, **138**, 2941–2944.
28 Z. Tan, J. Li, C. Zhang, Z. Li, Q. Hu, Z. Xiao, T. Kamiya, H. Hosono, G. Niu and E. Lifshitz, *Adv. Funct. Mater.*, 2018, **28**, 1801131.
29 B. W. Park, B. Philippe, X. Zhang, H. Rensmo, G. Boschloo and E. M. Johansson, *Adv. Mater.*, 2015, **27**, 6806–6813.
30 R. Nelson, K. Santra, Y. Wang, A. Hadi, J. Petrich and M. Panthani, *Chem. Commun.*, 2018, **54**, 3640–3643.
31 K. K. Bass, L. Estergreen, C. N. Savory, J. Buckeridge, D. O. Scanlon, P. I. Djurovich, S. E. Bradforth, M. E. Thompson and B. C. Melot, *Inorg. Chem.*, 2016, **56**, 42–45.
32 M. Gao, C. Zhang, L. Lian, J. Guo, Y. Xia, F. Pan, X. Su, J. Zhang, H. Li and D. Zhang, *J. Mater. Chem. C*, 2019, **7**, 3688–3695.
33 J. Zhang, Y. Yang, H. Deng, U. Farooq, X. Yang, J. Khan, J. Tang and H. Song, *ACS Nano*, 2017, **11**, 9294–9302.
34 B. Pradhan, G. S. Kumar, S. Sain, A. Dalui, U. K. Ghorai, S. K. Pradhan and S. Acharya, *Chem. Mater.*, 2018, **30**, 2135–2142.
35 M. B. Johansson, H. Zhu and E. M. Johansson, *J. Phys. Chem. Lett.*, 2016, **7**, 3467–3471.
36 M. Leng, Z. Chen, Y. Yang, Z. Li, K. Zeng, K. Li, G. Niu, Y. He, Q. Zhou and J. Tang, *Angew. Chem., Int. Ed.*, 2016, **55**, 15012–15016.
37 Y. Tang, M. Liang, B. Chang, H. Sun, K. Zheng, T. Pullerits and Q. Chi, *J. Mater. Chem. C*, 2019, **7**(11), 3369–3374.
38 Y. Lou, M. Fang, J. Chen and Y. Zhao, *Chem. Commun.*, 2018, **54**, 3779–3782.
39 Y. Zhang, J. Yin, M. R. Parida, G. H. Ahmed, J. Pan, O. M. Bakr, J.-L. Brédas and O. F. Mohammed, *J. Phys. Chem. Lett.*, 2017, **8**, 3173–3177.
40 B. Yang, J. Chen, F. Hong, X. Mao, K. Zheng, S. Yang, Y. Li, T. Pullerits, W. Deng and K. Han, *Angew. Chem., Int. Ed.*, 2017, **56**, 12471–12475.
41 M. Leng, Y. Yang, K. Zeng, Z. Chen, Z. Tan, S. Li, J. Li, B. Xu, D. Li and M. P. Hautzinger, *Adv. Funct. Mater.*, 2018, **28**, 1704446.
42 H. Yang, T. Cai, E. Liu, K. Hills-Kimball, J. Gao and O. Chen, *Nano Res.*, 2020, **13**, 282–291.
43 S. E. Creutz, H. Liu, M. E. Kaiser, X. Li and D. R. Gamelin, *Chem. Mater.*, 2019, **31**, 4685–4697.
44 L. Zhou, Y. F. Xu, B. X. Chen, D. B. Kuang and C. Y. Su, *Small*, 2018, **14**, 1703762.
45 C. B. Murray, S. Sun, W. Gaschler, H. Doyle, T. A. Betley and C. R. Kagan, *IBM J. Res. Dev.*, 2001, **45**, 47–56.
46 T. Paik, S.-H. Hong, E. A. Gaulding, H. Caglayan, T. R. Gordon, N. Engheta, C. R. Kagan and C. B. Murray, *ACS Nano*, 2014, **8**, 797–806.
47 J. Park, K. An, Y. Hwang, J.-G. Park, H.-J. Noh, J.-Y. Kim, J.-H. Park, N.-M. Hwang and T. Hyeon, *Nat. Mater.*, 2004, **3**, 891.
48 S. G. Kwon and T. Hyeon, *Small*, 2011, **7**, 2685–2702.
49 Y. w. Jun, J. s. Choi and J. Cheon, *Angew. Chem., Int. Ed.*, 2006, **45**, 3414–3439.
50 Y. C. Cao, *J. Am. Chem. Soc.*, 2004, **126**, 7456–7457.
51 L. Wu, S.-Y. Chen, F.-J. Fan, T.-T. Zhuang, C.-M. Dai and S.-H. Yu, *J. Am. Chem. Soc.*, 2016, **138**, 5576–5584.
52 S. E. Creutz, R. Fainblat, Y. Kim, M. C. De Siena and D. R. Gamelin, *J. Am. Chem. Soc.*, 2017, **139**, 11814–11824.
53 F. Wang, Y. Han, C. S. Lim, Y. Lu, J. Wang, J. Xu, H. Chen, C. Zhang, M. Hong and X. Liu, *Nature*, 2010, **463**, 1061.
54 F. T. Rabouw, P. T. Prins and D. J. Norris, *Nano Lett.*, 2016, **16**, 7254–7260.
55 L. Lian, G. Zhai, F. Cheng, Y. Xia, M. Zheng, J. Ke, M. Gao, H. Liu, D. Zhang and L. Li, *CrystEngComm*, 2018, **20**, 7473–7478.
56 V. F. Puntes, K. M. Krishnan and A. P. Alivisatos, *Science*, 2001, **291**, 2115–2117.
57 H. Huang, A. S. Susha, S. V. Kershaw, T. F. Hung and A. L. Rogach, *Adv. Sci.*, 2015, **2**, 1500194.
58 Y. Yang, Y. Jin, H. He, Q. Wang, Y. Tu, H. Lu and Z. Ye, *J. Am. Chem. Soc.*, 2010, **132**, 13381–13394.
59 H. Guo, Y. Chen, M. B. Cortie, X. Liu, Q. Xie, X. Wang and D.-L. Peng, *J. Phys. Chem. C*, 2014, **118**, 9801–9808.
60 J. Shamsi, Z. Dang, P. Bianchini, C. Canale, F. Di Stasio, R. Brescia, M. Prato and L. Manna, *J. Am. Chem. Soc.*, 2016, **138**, 7240–7243.

61 A. Pan, B. He, X. Fan, Z. Liu, J. J. Urban, A. P. Alivisatos, L. He and Y. Liu, *ACS Nano*, 2016, **10**, 7943–7954.
62 K. Wu, G. Liang, Q. Shang, Y. Ren, D. Kong and T. Lian, *J. Am. Chem. Soc.*, 2015, **137**, 12792–12795.
63 J. Li, L. Gan, Z. Fang, H. He and Z. Ye, *J. Phys. Chem. Lett.*, 2017, **8**, 6002–6008.
64 B. Yang, J. Chen, S. Yang, F. Hong, L. Sun, P. Han, T. Pullerits, W. Deng and K. Han, *Angew. Chem.*, 2018, **130**, 5457–5461.